ADVANCED ENERGY MATERIALS
www.advenergymat.de

Tuning Surface Rock-Salt Layer as Effective O Capture for Enhanced Structure Durability of $LiCoO_2$ at 4.65 V

Wangyang Ding, Hengyu Ren, Zijian Li, Mingjie Shang, Yongli Song, Wenguang Zhao, Liang Chang, Tianlu Pang, Shenyang Xu, Haocong Yi, Lin Zhou, Hai Lin, Qinghe Zhao, and Feng Pan**

Recently, the rock-salt (RS) phases are utilized to enhance the surface stability of $LiCoO_2$ (LCO), however, the optimization mechanism still remains vague. Herein, the structure stability of LCO is successfully enhanced via constructing a tough surface RS layer (≈5 nm), namely, the RS-LCO. This surface RS layer plays a significant role on capturing the migrated lattice O ions upon charging, leading to the progressive phase transition from an inert RS phase to an ionic conductive spinel phase in the surface, and suppresses the bulk H1-3 separation beyond 4.6 V. As a result, not only the oxygen redox induced side reactions are greatly reduced, but also the Li^+-ion's transport is significantly promoted. The RS-LCO/Li cells show a remarkable cycle stability with 89.7% capacity retention after 1000 cycles in 3–4.6 V at current of 1 C (1 C = 200 mA g^{-1}), and 81.2% capacity retention after 400 cycles in 3–4.65 V at 1 C. Besides, the RS-LCO/graphite cells show nearly no capacity decay in 600 cycles in 3–4.55 V at 1 C. This work provides a new insight to understand the role of surface RS phase layer on developing the advanced LCO.

1. Introduction

With the acceleration of 5G commercialization and continuous emergence of new electronic products, the demand for the lightweight and long lifespan batteries is proposed, thus the requirement for energy density of the key battery materials is further improved. $LiCoO_2$ (LCO) has long dominated the cathode materials in batteries of 3C products in the last 30 years.[1] To improve the energy density, the most feasible way is to increase the operating voltage of LCO.[1b,2] However, under a high operating voltage beyond 4.55 V versus Li/Li^+, the O3/H1–3 phase transition occurs with the less reversible sliding of Co–O slabs, leading to the lattice volume shrinkage, accumulated internal stress, microcracks, etc.[3] Comparing with the bulk, the surface structure damage is more severe.[4] The highly oxidative Co^{4+}/O^{n-} near the surface can induce an irreversible and harmful parasitic reaction between the surface structure and electrolyte, resulting in O loss, Co dissolution, and interface solvent decomposition.[5] Meanwhile, the surface will undergo structural degradation which is completely opposite to the LCO synthesis process, that is $LiCoO_2 \rightarrow Co_3O_4 \rightarrow CoO$, leading to a sharp increase in surface resistance.[6] This structural degradation process is always accompanied with a continuous O loss in the surface region of LCO.[5b,7] Thus, stabilizing the lattice O is crucial for the structure integrity and the suppression of side reactions.

Since the lattice O in layered structures is prone to loss upon high-voltage, the strategies utilizing the spinel (*Fd-3m*) and rock-salt (RS, *Fm-3m*) phases in surface region have been massively attempted to stabilize the lattice O in the near-surface zone of LCO.[8] Compared with the layered phase, the frameworks of spinel and RS phases are more stable with stronger covalent interaction between M (M represents the metal ions) and O, and thus can effectively stabilize the lattice O near the surface. Particularly, the RS phase presents the most closely-packed struc-

W. Ding, H. Ren, Z. Li, M. Shang, W. Zhao, S. Xu, H. Yi, L. Zhou, H. Lin, Q. Zhao, F. Pan
School of Advanced Materials
Peking University Shenzhen Graduate School
Peking University
Shenzhen 518055, China
E-mail: zhaoqh@pku.edu.cn; panfeng@pkusz.edu.cn

Y. Song
School of Energy and Power Engineering
Jiangsu University
Zhenjiang 212013, China

L. Chang
Institute of Materials Research
Tsinghua Shenzhen International Graduate School
Tsinghua University
Shenzhen 518055, China

T. Pang
National Key Laboratory of Materials for Integrated Circuits
Shanghai Institute of Microsystem and Information Technology
Chinese Academy of Sciences
Shanghai 200050, China

The ORCID identification number(s) for the author(s) of this article can be found under https://doi.org/10.1002/aenm.202303926

DOI: 10.1002/aenm.202303926

ture, and is usually composed of multiple foreign cations (such as Mg^{2+}, Ca^{2+}, Al^{3+}, La^{3+}, etc.) and anions (such as F^{-}, PO_4^{3-}, etc.), illustrating the infinite possibilities to modulate the surface chemistry.[9] Thus, understanding the structural properties of the surface RS phase layer is important for developing the next generation layered cathode materials.

Recently, our group has revealed the benefiting roles of surface RS phase on elevating the surface properties of LCO. First, we reported that the surface electric conductivity can be promoted by over one magnitude via constructing a coherent Al/F enriched RS phase on the surface of LCO.[10] Second, we revealed that the co-doping of surface Mg, Al, and Eu can induce a near-surface RS shell and a dopant segregation surface on LCO surface, leading to the suppressed O loss and reduced surface structure degradation.[11] Besides, Cai et al. also reported the utilization of (La, Ca)$CoO_{3-\delta}$ phase (similar to RS phase) to enhance the surface toughness of LCO at high voltage up to 4.8 V, serving as an oxygen buffer, and can reversibly uptake the O ions.[5b] Cheng et al. reported a surface modification involving a Zn-rich coating, a RS phase buffer layer, and a surface gradient Al doping layer, which reduced the detrimental issues of both side reactions and surface degradation of LCO at 4.6 V.[12] In above reports, the reinforced surface structures are attributed not only to the surface RS layers, but also to the foreign elements and surface coatings. Thus, the optimization mechanism of a pure surface RS layer is rarely reported in previous reports.

Herein, a tough RS layer with trace Si doping is successfully constructed on the surface of LCO, which is labeled as RS-LCO. Since the Si doping content is extremely trace (≈5 ppm), it can be regarded that the RS phase is mainly composed of the Li, Co, and O elements. Multiple characterizations and cell tests are conducted and analyzed, and the obtained results indicate that, the homogeneous surface RS phase layer on LCO first plays a significant role on inhibiting the surface O loss, reducing side reactions and surface structural deterioration, and then effectively suppressing the H1-3 separation process in the bulk, reducing the crack's generation inside the LCO. Besides, for the first time, we reveal a completely opposite surface phase evolution process occurring on RS-LCO upon cycles, that is, a phase transition from "RS to spinel", mainly via capturing the migrated active O from the subsurface structure of RS-LCO. This gradual "RS to spinel" phase transition in the surface region contributes to a capacity activation process, and forms an ionic conductive and tough surface spinel layer for the enhanced cycle and rate performances of RS-LCO. As a result, the RS-LCO/Li cells show a remarkable cycle stability with 89.7% capacity retention after 1000 cycles in 3–4.6 V at current of 1 C, and 81.2% capacity retention after 400 cycles in 3–4.65 V at 1 C. This work provides a new insight to understand the benefit roles of surface RS phases, and will guide the design and synthesize of the next-generation layered cathode materials.

2. Results and Discussion

2.1. Material Characterizations

Constructing a protective RS surface layer has been proved to be effective on enhancing the structure stability of LCO upon high voltage. In previous reports, the obtained RS surface layers are usually enriched with some foreign inert elements, such as the Mg–Al–Eu,[11] Al–F,[10] Zn–Al,[12] etc. In other words, the formation of surface RS layers requires the assistance of these foreign elements. In this study, a tough RS layer is achieved on surface of a pure LCO (P-LCO) mainly via introducing trace amount of Si doping (≈5 ppm), namely, the RS-LCO. The applied surface Si source comes from the tetraethyl orthosilicate ($C_8H_{20}O_4Si$), which produces the highly dispersed $Si(OH)_4$ colloids in a hot water (≈90 °C) through hydrolysis, and uniformly coats on the LCO surface. The $Si(OH)_4$ coated LCO is then sintered at a medium temperature of 600 °C in air atmosphere to obtain RS-LCO. The detailed synthesize method is shown in Supporting Information.

X-ray diffraction (XRD) measurements are conducted to reveal the phase structure of the LCO cathodes, as shown in **Figure 1a** and Figure S1 (Supporting Information). For both samples, all the diffraction peaks can be well indexed to the layered α-$NaFeO_2$ structure with a space group of *R-3m*. Further, the XRD refinement results present nearly the same lattice parameters for both P-LCO and RS-LCO, indicating that the surface treatment has no influence to the bulk structure of LCO. The surface morphology of LCO is characterized by the scanning electron microscope (SEM) (Figure 1b; Figure S2, Supporting Information). The results indicate that, the trace Si-doping presents no change to the surface morphology of LCO. The X-ray photoelectron spectroscopy (XPS) measurements are applied to examine the existence of surface Si doping in the surface region of RS-LCO (Figure S3, Supporting Information). For RS-LCO, obvious signals of Si 2s spectra can be detected around binding energy of 153.4 eV,[13] and the diffusion depth of Si doping in surface of RS-LCO is beyond 50 nm, while for P-LCO, no signals of Si 2s spectra can be detected. In other words, there exists the gradual Si doping in the surface structure of RS-LCO. For O 1s spectra peaks, the Si─O bonds is detected on surface of RS-LCO (Figure S4, Supporting Information), locating with binding energy of 530.6 eV.[14] Besides, the surface Si doping can be further identified by the energy dispersive spectrometer (EDS) mapping of both the surface and cross-section morphology results (Figures S5 and S6, Supporting Information).

We further apply the transmission electron microscope (TEM) to probe the phase structure on surface of RS-LCO (Figure 1c). The surface RS layer can be clearly identified with a thickness of ≈5 nm, and the fast Fourier transform (FFT) results also show the diffraction patterns of both the surface RS phase (zone I) and the layered phase (zone II), showing that the surface Si doping can promote the formation of RS phase. To identify the promoting effect of surface Si doping, the LCO without surface Si doping is synthesized, that is, P-LCO is simply treated via a hot water, and then sintered at 600 °C in air atmosphere (Figure S7a, Supporting Information), namely, the H-LCO. The result shows a hybrid of RS and layered phases in the surface region of H-LCO, rather than a pure RS phase layer. For P-LCO, the surface structure is mainly featured a layered phase (Figure S7b, Supporting Information). Besides the differences in phase structures, the existence states of Li, Co, and O in the surface RS layer are very different from that in the bulk. The electron energy-loss spectroscopy (EELS) spectra measurements are applied to characterize the O K-edge, Li K-edge, and Co L-edge in the surface of RS-LCO (Figure 1d). The signal of Li K-edge is weak within a depth of ≈5 nm, and gradually strengthens as the depth

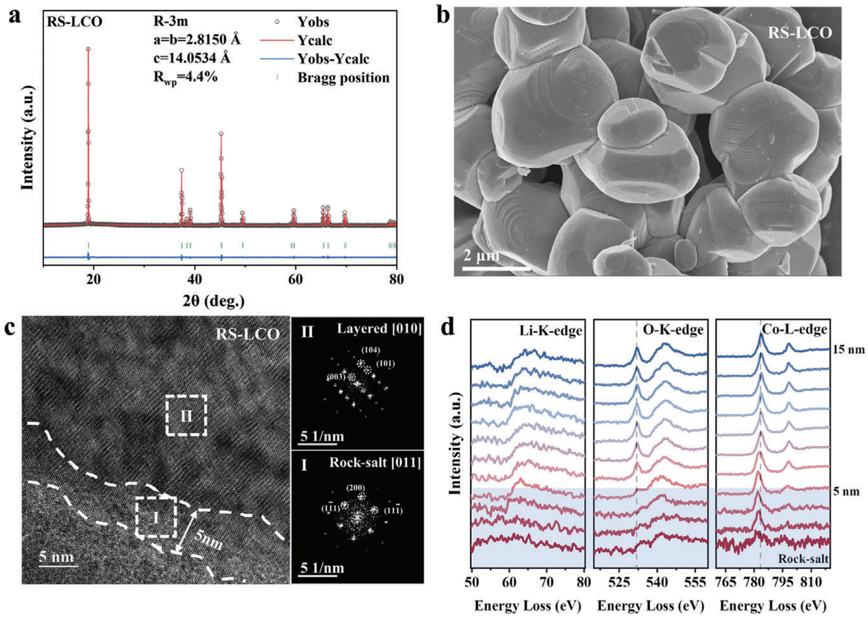

Figure 1. Material characterizations. a) XRD pattern and b) SEM morphology of RS-LCO. c) TEM cross-section morphology and corresponding diffraction patterns of RS-LCO. d) EELS spectra results of Li K-edge, O K-edge, and Co L-edge from surface to interior of RS-LCO.

increases from surface to interior, indicating that the surface RS layer is in a Li-deficient state. For O K-edge peaks, the diminished O pre-peaks in the surface region of RS-LCO refers to the occurrence of new phase similar to CoO, which is a typical RS phase.[15] For Co L_3-edge, comparing with the bulk, a slight shift to lower energy loss is observed in the surface region, showing a Co^{2+}(major)/Co^{3+}(minor) valence state.[16] In addition, the formation of surface RS phase can be further confirmed by the Raman spectroscopy results in Figure S8 (Supporting Information). Combining the results above, the surface RS layer of RS-LCO is successfully constructed, and presents a Li^+-deficient and Co^{2+}-dominated character.

2.2. Electrode Performances

The LCO/Li cells are assembled and tested to explore the enhanced electrode performances of RS-LCO. **Figure 2a–c** compare the charge/ discharge curves in the initial three cycles at a current of 0.2 C (1 C = 200 mA g^{-1}), and the rate performances (0.2–16 C) of P-LCO and RS-LCO cathodes, in potential range of 3–4.6 V. For P-LCO, the charge/discharge curves overlap well in the initial three cycles, which is very different from that of RS-LCO. For RS-LCO, a capacity activation (CA) process is obviously observed, as identified by the gradually increased discharge capacities in the initial cycles. We consider that, this CA process is closely related to the gradual phase evolution of the surface RS phase upon cycles, and it reappears even when the operating potential range expands to 3–4.65 V (Figure S9, Supporting Information). We also observe that, comparing with P-LCO, the RS-LCO presents higher coulombic efficiency (CE) values in the initial three cycles (Figure S10, Supporting Information), mainly due to the fewer side reactions on surface of RS-LCO. Besides, the existence of the surface RS layer also elevates the rate performances. At a high rate of 16 C, the RS-LCO shows a high capacity delivery of 156 mAh g^{-1}, which is much higher than that of P-LCO with only 52 mAh g^{-1} at 16 C.

The cycle stability is the most important performance index for evaluating the cathode materials.[17] Figure 2d,e and Figure S11 (Supporting Information) compare the cycle performances and voltage profiles of P-LCO and RS-LCO cathodes at 1 C, and in the potential ranges of 3–4.6 V and 3–4.65 V, respectively. The results indicate that, the RS-LCO shows a high capacity retention of 89.7% after 1000 cycles in 3–4.6 V, and a high capacity retention of 81.2% after 400 cycles in 3–4.65 V, which is among the best reported high-voltage LCO cathodes (Table S1, Supporting Information). As a comparison, the cycle stability of P-LCO is obviously inferior than that of RS-LCO. The cycle stability of RS-LCO is further evaluated at 5 C (Figure S12a, Supporting Information), showing a high capacity retention of 93% after 1000 cycles in 3–4.6 V. Furthermore, the RS-LCO/graphite full-cells are also assembled and cycled at 1 C, and in a potential range of 3–4.55 V, which exhibits an excellent cycle stability with nearly no capacity decay in 600 cycles (Figure S12b, Supporting Information), and these cells are still running well. The above results indicate that, the cycle and rate performances of RS-LCO can be greatly enhanced by constructing a tough surface RS layer. It is noted that, the capacity activation of RS-LCO, correlating to the gradual surface phase evolution upon cycles, plays a significant role on elevating the electrode performances, which will be discussed in the following parts.

2.3. Suppressed H1−3 Separation

The obviously enhanced cycle and rate performances of RS-LCO are closely related to the optimized structure evolution process in both the bulk and surface.[1a] For the bulk structure, once

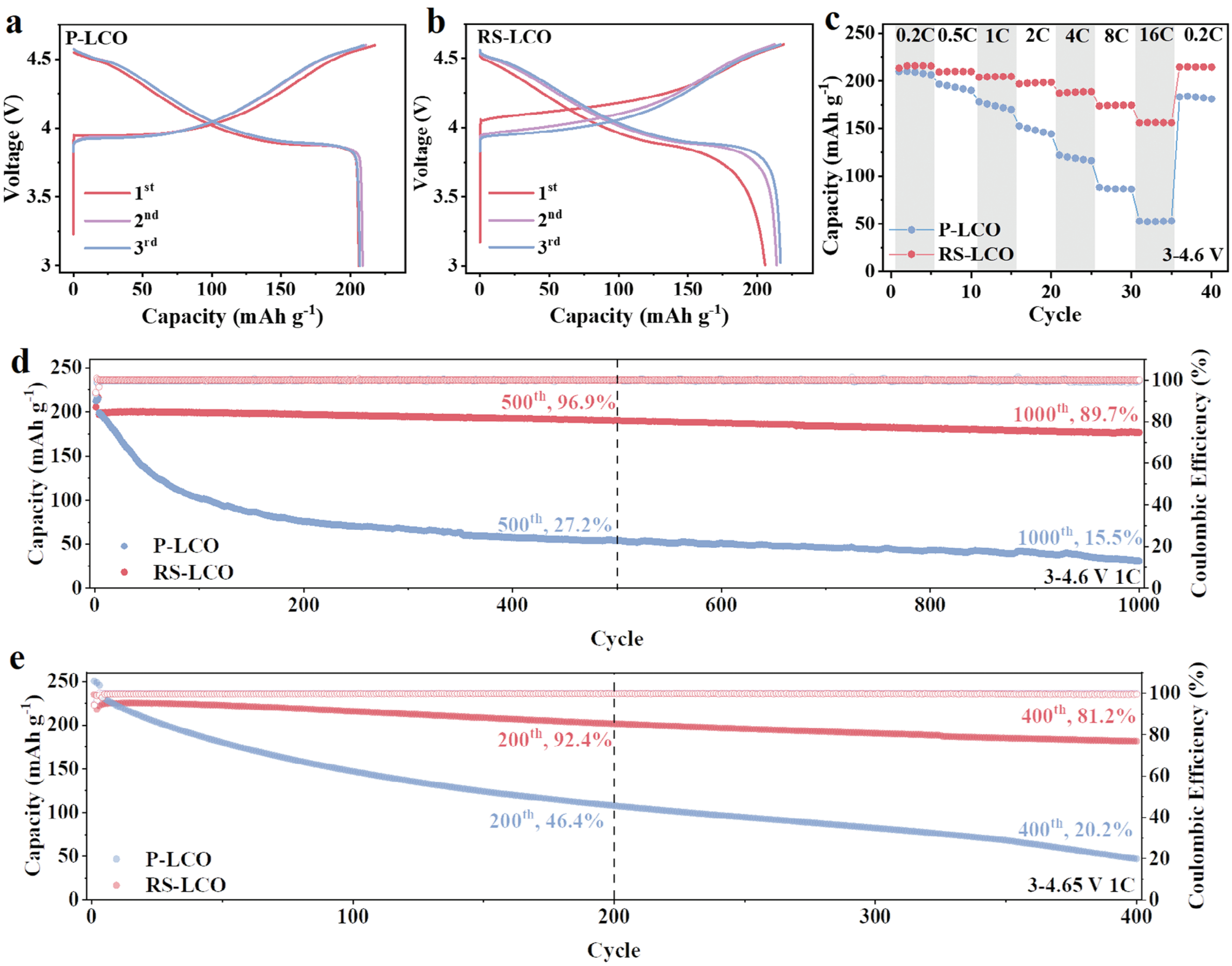

Figure 2. Electrode performances. Comparison of charge/discharge curves of a) P-LCO/Li and b) RS-LCO/Li cells at current of 0.2 C, in voltage range of 3–4.6 V. c) Comparison of rate performances of P-LCO and RS-LCO. Comparison of long-term performances of P-LCO and RS-LCO within d) 3–4.6 V and e) 3–4.65 V.

charged to beyond 4.55 V, the O3/H1-3 phase transition occurs with the shrinkage of the lattice volume, triggering the internal stress, which gradually accumulates into the microcracks, and eventually leads to the bulk failure.[18] Thus, suppressing the irreversible O3/H1-3 phase transition is vital for enhancing the cycle stability of LCO. The in situ XRD patterns are utilized to reveal the phase evolution of P-LCO and RS-LCO in a potential range of 3–4.6 V, and at current of 0.3 C (**Figure** 3a,c). Generally, the shift of (003) peaks (Δ2Θ) represents the layer spacing variations of the Co–O layers. However, according to the in situ XRD patterns, the content of O1a phase is much lower than H1-3 phase at the highly delithiated state, which can not represent the overall lattice variations. Therefore, we define the values of Δ2Θ as the shift of main peak position. As a comparison, the Δ2Θ values are 0.806° and 0.634° for P-LCO and RS-LCO, respectively, showing the suppressed lattice variation of RS-LCO. Comparing the variation of (101) peaks, for RS-LCO, fewer O1a phase (the separated O1 phase inside the H1-3) is observed when charged to 4.6 V, while for P-LCO, the generation of O1a phase appears obviously, indicating more H1-3 separation in P-LCO.

In Figure 3b,d, we compare the H1-3 separation behavior of P-LCO and RS-LCO after charged to 4.56, 4.58, and 4.6 V, respectively. When charged beyond 4.56 V, the (003) peaks can be separated and fitted in three parts, including the O3, H1-3, and O1a phases, which is located at 2Θ of 18.6°, 19.0°, and 19.6°, respectively. It is noted that, for P-LCO, once charged beyond 4.56 V, the O3 phase completely disappears, while for RS-LCO, the O3 phase preserves until to 4.6 V, indicating that the surface RS layer can delay the phase transitions from "O3 to H1-3, then to O1a", leading to the higher bulk structure stability of RS-LCO. We further observe that, after charged to 4.6 V, the median peak width of RS-LCO is obviously larger than P-LCO, indicating the short-range ordered character of the H1-3 phase in RS-LCO. Upon discharging, this short-range ordered H1-3 phase is more preferred to transform back the O3 phase, thus enabling a high phase transition reversibility of RS-LCO. Due to the delayed effect on the O3/H1-3 phase transition and the suppressed H1-3 separation

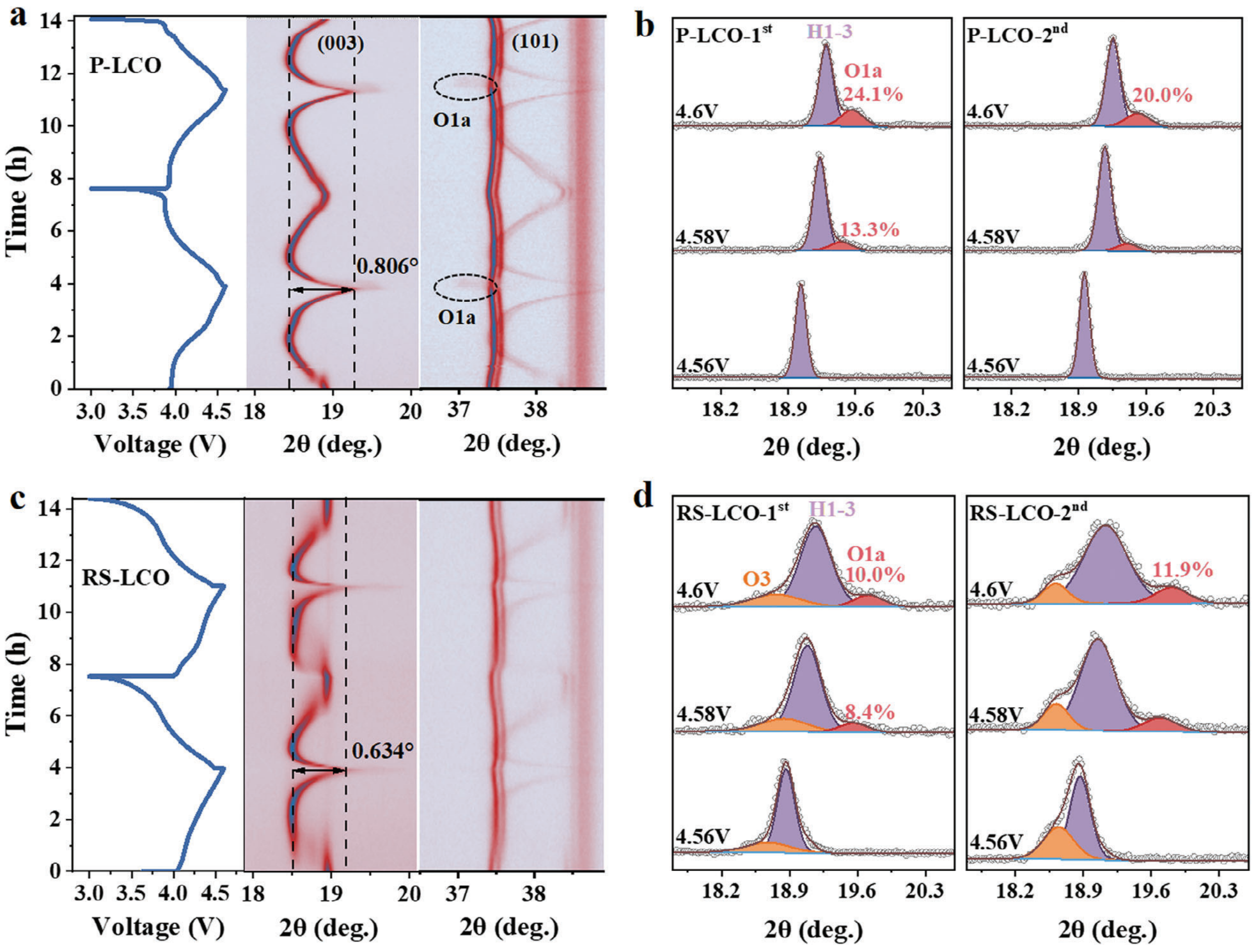

Figure 3. XRD analyses of the bulk phase evolution. The in situ XRD patterns of a) P-LCO, and c) RS-LCO in the initial two cycles within 3–4.6 V. Analyses of the H1-3 separation of b) P-LCO and d) RS-LCO cathodes in the 1st and 2nd cycles.

in the bulk RS-LCO, the proportion of O1a phase in RS-LCO is obviously lesser than that in P-LCO. The comparison of bulk structures of P-LCO and RS-LCO after charged to 4.6 V in the 1st cycle is further presented in Figure S13 (Supporting Information). For P-LCO, serious lattice distortions and considerable "layered to spinel" phase transition is observed in the bulk, while for RS-LCO, the bulk structure presents a relatively intact layered structure, demonstrating the reinforced stability of layered structure for RS-LCO. Due to the more stabilized layered structure, the crack's formation in the bulk is effectively prevented. Figure S14 (Supporting Information) compares the cross-section of P-LCO and RS-LCO after 1000 cycles in 3–4.6 V and at 1 C. The cracks are obviously observed inside the P-LCO particles, while for RS-LCO, nearly no visible cracks are observed, indicating the obviously suppressed crack's generation by the surface RS layer.

2.4. Surface RS/Spinel Phase Evolution

Upon charging, part of the Li^+ ions inside the LCO particles can be extracted, and dissolves into the electrolyte.[19] Since the surface region of pristine RS-LCO is Li-deficient, the Li^+ ion's migration across this Li-deficient surface inevitably cause the structure rearrangement. Revealing this in situ structure rearrangement process is significant to understand the enhanced cycle and rate performances of RS-LCO. Cyclic voltammetry (CV) tests are usually applied to reveal the structural electrochemistry in the surface of LCO.[20] In Figure S15 (Supporting Information), the CV curves of LCO/Li cells in the initial 20 cycles are performed with a scanning rate of 0.2 mV s^{-1}, and in a potential range of 3–4.65 V. For RS-LCO, the oxidative CV peaks show a sudden left shift from the 1st to 2nd cycle, and then gradually left shift from the 2nd to 20th cycle, reflecting the gradual surface phase evolution upon cycles. However, for P-LCO, the oxidative CV peaks first gradually left shift from the 1st to 9th cycles, then gradually right shift from the 10th to 20th cycles, with the gradually decreased peak intensities and increased peak width, indicating a progressive phase deterioration in the surface.

The surface phase evolution can be identified via TEM characterizations (Figure S16, Supporting Information), which compares the surface structures of both the RS-LCO and P-LCO after the initial two cycles. The results indicate that, for RS-LCO, part of the surface RS phase has transformed to Spinel phases, while for P-LCO, the pristine layered structure in the surface has completely transformed into the Spinel phases. Generally, for a pure

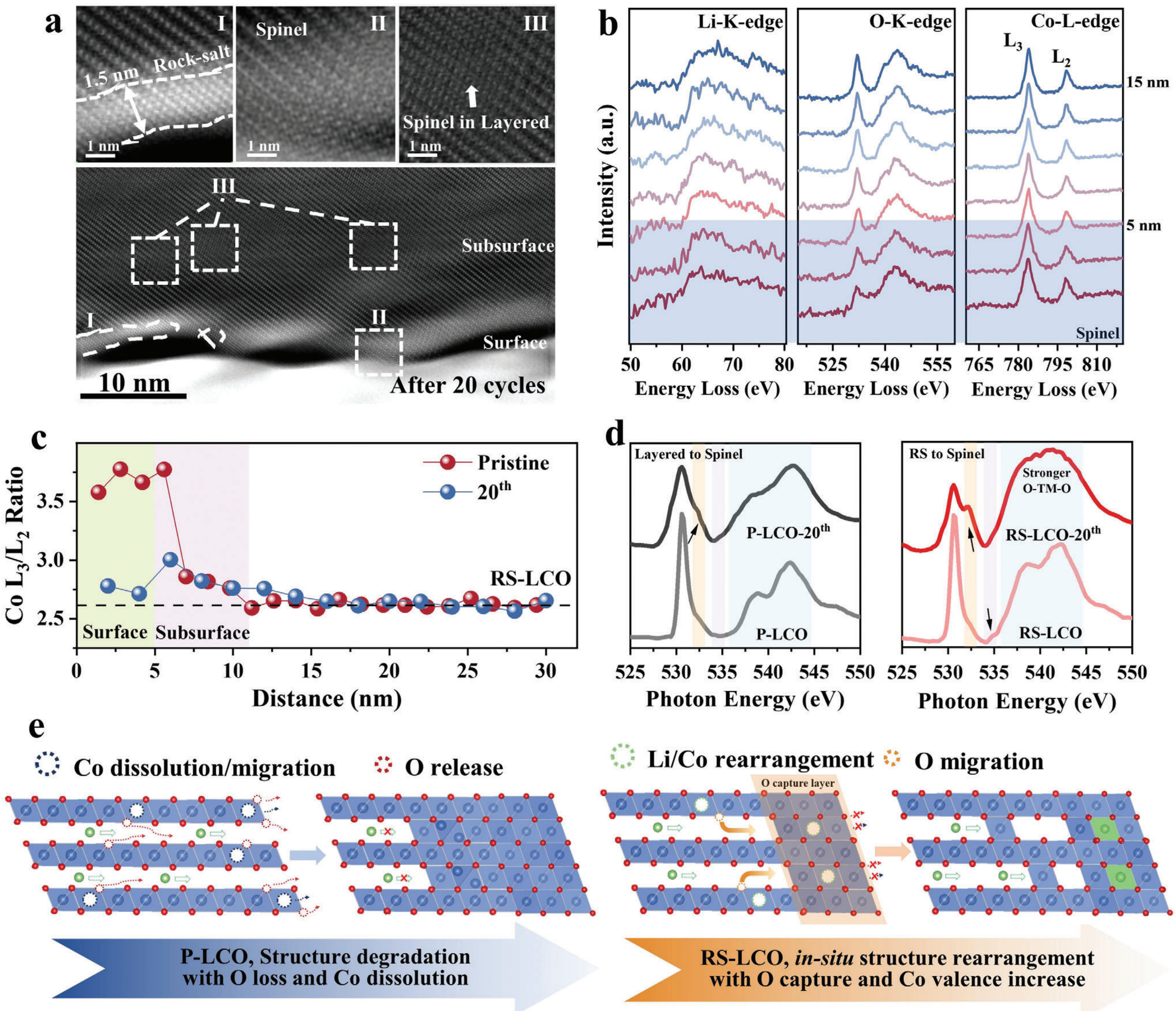

Figure 4. Revealing the "RS to Spinel" phase transition via capturing active O. a) TEM characterization of surface structure of RS-LCO after 20 cycles at 1 C, and b) the correlated EELS spectra results in the surface region. c) Comparison of the Co L_3/L_2 ratio in the surface of the RS-LCO at pristine state and after 20th cycles at 1 C. d) sXAS spectra results of RS-LCO and P-LCO at pristine state and after 20th cycles at 1 C. e) Schematic diagrams of the surface structure evolution for the P-LCO and RS-LCO.

layered surface structure, upon high-voltage cycle, the phase transition usually evolves from "Layered to Spinel, and eventually to RS" with the continuous loss of lattice O from the oxygen framework of LCO.[21] However, this work presents an opposite phase evolution from "RS to Spinel" on the surface of RS-LCO. Since the phase evolution from RS (typically, CoO phase) to Spinel (typically, $Li_xCo_2O_4$ phase) requires additional lattice O,[6c,22] revealing the origin of this additional lattice O is the key for understanding the enhanced electrode performance. **Figure 4a** shows the surface phase structure of the RS-LCO after the 20th cycle. We observe that, on the outermost surface, only small part of RS phases retains with a thickness of <2 nm (region I), and the major part of the surface has converted to a pure Spinel phase (region II). We speculate that, the lattice O required for the "RS to Spinel" transition comes from the lattice framework in the subsurface of RS-LCO (region III). In region III, the Spinel phase can be detected mixing with the original layered phase. The above results clearly show that, the lattice O can migrate from the subsurface region to the surface region upon cycles beyond 4.6 V, resulting in the successful "RS to Spinel" transition in the surface regions, and the "Layered to Spinel" transition in the subsurface regions. As a result, the O_2 release is suppressed due to the active O capture by surface RS, thus enables a stable Co–O lattice framework upon cycles.

The reinforced structure stability can be further identified by the EELS and the soft X-ray absorption spectroscopy (sXAS) spectra results of the cycled LCO. Figure 4b shows the EELS spectra results of the Li K-edge, O K-edge, and Co L-edge in the surface of RS-LCO after the 20th cycle. It can be seen that, after 20 cycles, the Li-deficient state in the surface of RS-LCO disappears, as identified from the Li K-edge spectra. Besides, the pre-peaks of O K-edge spectra at energy loss of 531.6 eV appears, and the peak shift of the Co L-edge spectra disappears in the surface region, mainly attributing to the phase transition from RS to Spinel. Accompanying with the surface phase transition, the Co valence in the surface regions is also increased. Figure 4c compares the variation of Co L_3/L_2 ratios from surface to interior (within a depth of 30 nm) of RS-LCO samples at the pristine state and after 20 cycles, respectively. The lower the Co L_3/L_2 ratios, the higher the valence of Co in the surface of RS-LCO.[23] It can be seen that, the surface Co valence is increased due to the phase transition from RS to Spinel. Figure 4d shows the O K-edge spectra of TEY mode from sXAS measurements of P-LCO and R-LCO, at the pristine and after 20th cycle, respectively. For P-LCO, the traditional phase transition process from layered (Co^{3+}) to Spinel (Co^{n+}, 2<n<3) occurs. Specifically, in pristine P-LCO, the peak located at photon energy of 530.5 eV corresponds to the Co^{3+}(eg) – O 2p hybridization states.[21] After 20th cycle, a higher angle shoulder peak (photon energy of 532.2 eV) is observed, which is assigned to the low Co valence Spinel (typically, the Co_3O_4).[24] For RS-LCO, the opposite phase transition from “RS to Spinel” is visually monitored. Specifically, the transition from RS phase (Co^{2+}(major)/Co^{3+}(minor) mixed state with higher photon energy of 534.7 eV) to Spinel phase (Co^{n+}, 2<n<3, photon energy of 532.2 eV) occurs via capturing active lattice O from subsurface.[15,25] Besides, we further observe that, the characteristic peaks within the photon energy of 535–545 eV are wider and higher in RS-LCO, which corresponds well to the stronger O 2p-TM 4s/4p interaction,[2,26] and is conducive to the formation of a more stable O skeleton.

Combing the CV curves, TEM characterizations, EELS spectra, and sXAS spectra results, the mechanism of this gradual “RS to Spinel” phase transition in the surface region of RS-LCO is revealed, as illustrated in Figure 3e. During synthesize, a tough RS layer is pre-fabricated on the surface of RS-LCO. Inside this Li-deficient RS layer, the Co valence is at a Co^{2+}(major)/Co^{3+}(minor) mixed state. Upon charging, the Li^+ ions are extracted from the bulk across this RS layer, which brings additional Li^+ ions, increases the Co valence from $Co^{2+/3+}$ to $Co^{3+/4+}$, and also captures the migrated O from the subsurface region. Upon discharging, due to the intercalated Li^+ ions and the captured O, part of the surface RS phase transforms to the Spinel phase (typically, the $Li_xCo_2O_4$ phase). This “RS to Spinel” phase transition is a progressive process, and after certain amount of cycles, all the RS phase in the surface transform to the Spinel phase. This particular “RS to Spinel” phase transition enables an enhanced cycle and rate performances of RS-LCO. However, for P-LCO with pure layered surface structure, the serious O loss and Co dissolution issues causes serious surface structure deterioration, leading to the gradual phase transition from “Layered to Spinel, and eventually to RS” with serious capacity decay.

2.5. Reduced Side Reactions and Enhanced Li

Reduced Side Reactions and Enhanced Li^+In above discussions, we reveal the role of surface RS layer on capturing the migrated O from the subsurface. Here, we further clarify the interface reactions between the surface RS layer and electrolyte, and the Li^+ ion transport kinetics across this surface RS layer. When charged to a high voltage beyond 4.6 V, the highly oxidative Co^{4+} and $O^{\alpha-}$ ($0<\alpha<2$) ions occur, and oxidize the solvents, such as EC, EMC, FEC, etc., resulting in the gas release, including the O_2, CO_2, and CO, etc.[27] Thus, the gas release can be the index for evaluating the interface side reactions. The differential electrochemical mass spectrometry (DEMS) tests are performed to probe the gas release from the LCO/Li cells in the initial three cycles, in 3–4.65 V and at 0.3 C (**Figure 5a,b**). The gas release from RS-LCO/Li cells is obviously lesser than that from P-LCO/Li cells, indicating the fewer side reactions. Notably, the O_2 release from RS-LCO/Li cells is very low throughout the entire testing process, mainly attributing to the beneficial effect on capturing the active O by the surface RS phase.

The different side reactions lead to the different cathode electrolyte interface (CEI) products on surfaces of P-LCO and RS-LCO (Figure S17, Supporting Information). For RS-LCO, a homogeneous and compact CEI layer is detected on the surface with a thickness of ≈9 nm, while for P-LCO, the CEI layer is thick and porous with a thickness of 130 nm. From the morphology aspect, the CEI layer on RS-LCO seems to be more protective than that on P-LCO. Chen's group has contributed this optimized CEI layer to the altered abundant species in inner Helmholtz layer (IHL) of the LCO surface.[8a] Here, due to the passivation effect of the surface RS layer, a PF_6^- enriched IHL can be achieved after charging, enabling the formation of the inorganic-rich CEI. The compositions of CEI layers are analyzed by XPS (Figure S18, Supporting Information). The F 1s peaks can be separated into three peaks, including $Li_xPO_yF_z$, and LiF, locating at binding energies of 686.6 and 685.1 eV, respectively.[5a,28] The O 1s peaks can be separated into six peaks, including the lattice O, R-OLi, P-O, C-O, C=O, and $Li_xPO_yF_z$, locating at the binding energies of 529.8, 530.4, 531.2, 532.0, 532.9, and 534.1 eV, respectively.[29] The $Li_xPO_yF_z$ content in CEI of RS-LCO is obviously lesser than P-LCO, indicating the lesser decomposition of $LiPF_6$ salts. Besides, the organic compounds in CEI of RS-LCO is also lesser than P-LCO, indicating the lesser decomposition of solvents, which is consistent with the DEMS results in Figure 5a,b. This significant difference in CEI layer retains even after 1000 cycles in 3–4.6 V and at current of 1 C (Figures S19 and S20, Supporting Information).

The above results clearly demonstrate the obviously optimized surface structure and CEI layers of RS-LCO, which enables a rapid and stable Li^+ insertion/ extraction upon cycles. The elevated rate performance of RS-LCO can be regarded as a result of the promoted Li^+ ion transport kinetics, which can be further evaluated by the galvanostatic intermittent titration technique (GITT) tests (Figure S21, Supporting Information),[30] and the calculated Li^+ diffusion coefficient (D_{Li+}) are shown in Figure 5c. The results indicate that, in the 1st charging process, the D_{Li+} values of RS-LCO are obviously lower than P-LCO, mainly attributing to the Li^+-deficient property of the surface RS layer. While in the 1st discharging process and in the 2nd cycle, the D_{Li+} values of RS-LCO are obviously higher than P-LCO, which illustrates the enhanced Li^+ ion diffusion kinetics across the surface due to the successful “RS to Spinel” transition.

The electrochemical impedance spectroscopy (EIS) are further conducted to analyze the enhanced performance of RS-LCO

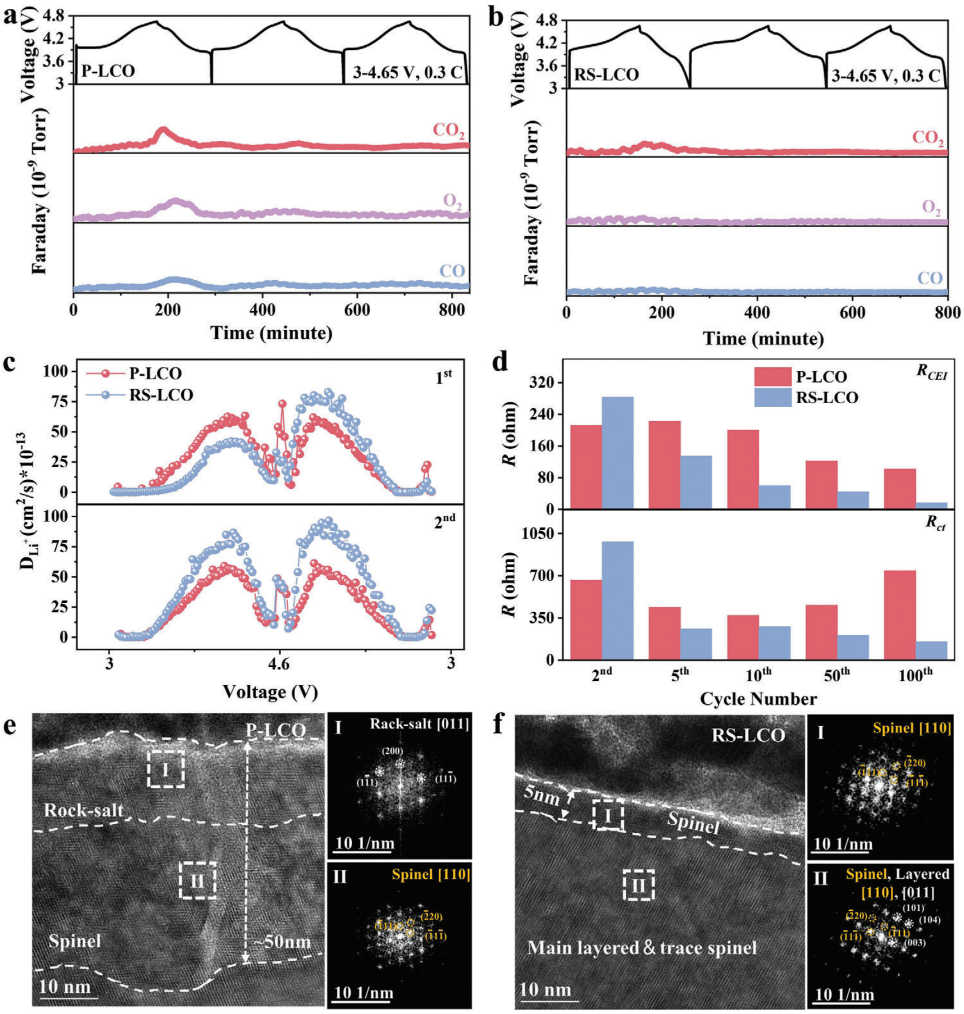

Figure 5. Surface side reactions, Li^+ ion transport kinetics, and the surface structure evolution of P-LCO and RS-LCO. Comparison of the DEMS measurements of a) P-LCO/Li and b) RS-LCO/Li cells in 3–4.65 V and at current of 0.3 C. Comparison of c) diffusion kinetics in initial two cycles and d) the R_{CEI} and R_{ct} values from the 2nd to 100th cycles of P-LCO and RS-LCO. Comparison of the surface structure characterizations of e) P-LCO and f) RS-LCO after 1000 cycles in 3–4.6 V and at current of 1 C.

(Figure S22, Supporting Information). Generally, upon cycles, the LCO interface structure composes the CEI layer on the surface, the phase transition layer (PTL) in the surface, and the layered structure in the bulk.[19] Upon Li^+ insertion, the Li^+ ions diffuse successively across the CEI, the PTL, finally enter into the bulk, and vice versa for the Li^+ extraction process. As reflected in a typical EIS plots, two impedance semicircles and one diffusion tail correspond to the resistance of CEI, the PTL, and the Li^+ ion diffusion inside the bulk, respectively.[31] Among which, the resistance of CEI and PTL are abbreviated as the R_{CEI} and R_{ct}, respectively.[32] The fitted results of the R_{CEI} and R_{ct} after 2nd, 5th, 10th, 50th, and 100th cycles are presented in Figure 5d. It is observed that, for two samples, the R_{CEI} values decrease gradually as it proceeds from the 2nd to 100th cycles, mainly due to the gradually enhanced ionic conductivity of CEI layers upon cycles.[33] Further, the R_{CEI} values of RS-LCO are obviously lower than P-LCO, mainly due to the thin and homogeneous feature of CEI layer on surface of RS-LCO. Besides, the R_{ct} values of RS-LCO decreases gradually from the 2nd to 100th cycles, mainly attributing to the "RS to Spinel" phase transition, which promotes the formation of the highly ionic conductive Spinel-type $Li_xCo_2O_4$. While for P-LCO, the R_{ct} values increase from 10th to 100th cycles, which corresponds to the detrimental surface structure deterioration due to the continuous O loss and Co dissolution from the surface.

The difference in the R_{ct} values of P-LCO and R-LCO represent the different characters of surface PTL properties. TEM characterizations are applied to reveal the surface structures of LCO after 1000 cycles in 3–4.6 V, and at 1 C (Figure 5e,f). For P-LCO, we observe an obvious RS phase layer in the surface with thickness of ≈15–20 nm, and a Spinel phase layer in the subsurface with thickness of ≈30–40 nm, indicating a serious surface structure deterioration. This kind of structure deterioration in the surface is mainly attributed to the continuous O loss and Co dissolution upon long-term cycles, and is responsible for the serious capacity decay. As for RS-LCO, there is only a thin Spinel phase layer in the surface region, which is transformed from the original RS layer in the surface. Figure S23 (Supporting Information) compares the XPS Co 2p signals on the Li anodes of LCO/Li cells after 1000 cycles in 3–4.6 V and at 1 C. For RS-LCO, no Co dissolution is observed, while for the P-LCO, obvious Co dissolution issue is identified. Therefore, for RS-LCO, the pre-fabricated surface RS layer not only reduces the side reactions, promotes to form a homogeneous and thin CEI layer, but also enables an elevated Li^+ ion's transport kinetics via forming a highly ionic conductive surface Spinel (i.e., the $Li_xCo_2O_4$) phase. The root cause for the multiple effects is mainly attributed to the role of surface RS layer on capturing the active O, which traps the active O and reduces the Co dissolution, thus enables a stabilized surface structure for both the enhanced cycle and rate performances of RS-LCO.

3. Conclusion

In summary, this work reveals a novel surface RS phase layer as effective O capture to enhance the structure durability of RS-LCO. Upon charging, the homogeneous surface RS phase layer on RS-LCO plays a significant role on capturing the migrated O ions from the subsurface regions, and gradually transforms to a Spinel phase. This progressive "RS to Spinel" phase transition not only reduces the O release from surface of RS-LCO, but also leads to the formation of surface Spinel phase with an enhanced Li^+ ion's transport kinetics. Benefited from the reduced O release, the side reactions are greatly reduced, and the surface Co–O lattice structure is also largely stabilized, which significantly enhances the cycle stability of RS-LCO. The RS-LCO/Li cells show a remarkable cycle stability with 89.7% capacity retention after 1000 cycles in 3–4.6 V at current of 1 C (1 C = 200 mA g^{-1}), and 81.2% capacity retention after 400 cycles in 3–4.65 V at 1 C, and the RS-LCO/graphite full cells show nearly no capacity decay in 600 cycles in 3–4.55 V at 1 C, which is among the best reported high-voltage LCO cathodes.

Supporting Information

Supporting Information is available from the Wiley Online Library or from the author.

Acknowledgements

W.D. and H.R. contributed equally to this work. This work is financially supported by the National Natural Science Foundation of China (No. 52102201), the National Natural Science Foundation of China (No. 52102200), and the Basic and Applied Basic Research Foundation of Guangdong Province (No. 2021B1515130002).

Conflict of Interest

The authors declare no conflict of interest.

Data Availability Statement

Research data are not shared.

Keywords

$LiCoO_2$, oxygen release, phase transition, rock-salt phase, structure stability

Received: November 17, 2023
Revised: December 16, 2023
Published online: January 2, 2024

[1] a) J.-N. Zhang, Q. Li, C. Ouyang, X. Yu, M. Ge, X. Huang, E. Hu, C. Ma, S. Li, R. Xiao, W. Yang, Y. Chu, Y. Liu, H. Yu, X.-Q. Yang, X. Huang, L. Chen, H. Li, *Nat. Energy* **2019**, *4*, 594; b) Q. Liu, X. Su, D. Lei, Y. Qin, J. Wen, F. Guo, Y. A. Wu, Y. Rong, R. Kou, X. Xiao, F. Aguesse, J. Bareño, Y. Ren, W. Lu, Y. Li, *Nat. Energy* **2018**, *3*, 936.
[2] J. Chen, H. Chen, S. Zhang, A. Dai, T. Li, Y. Mei, L. Ni, X. Gao, W. Deng, L. Yu, G. Zou, H. Hou, M. Dahbi, W. Xu, J. Wen, J. Alami, T. Liu, K. Amine, X. Ji, *Adv. Mater.* **2022**, *34*, 2204845.
[3] a) H. Ren, W. Zhao, H. Yi, Z. Chen, H. Ji, Q. Jun, W. Ding, Z. Li, M. Shang, J. Fang, K. Li, M. Zhang, S. Li, Q. Zhao, F. Pan, *Adv. Funct. Mater.* **2023**, *33*, 2302622; b) A. Van Der Ven, M. K. Aydinol, G. Ceder, *J. Electrochem. Soc.* **1998**, *145*, 2149.
[4] J. Li, C. Lin, M. Weng, Y. Qiu, P. Chen, K. Yang, W. Huang, Y. Hong, J. Li, M. Zhang, C. Dong, W. Zhao, Z. Xu, X. Wang, K. Xu, J. Sun, F. Pan, *Nat. Nanotechnol.* **2021**, *16*, 599.
[5] a) W. Huang, Q. Zhao, M. Zhang, S. Xu, H. Xue, C. Zhu, J. Fang, W. Zhao, G. Ren, R. Qin, Q. Zhao, H. Chen, F. Pan, *Adv. Energy Mater.* **2022**, *12*, 2200813; b) M. Cai, Y. Dong, M. Xie, W. Dong, C. Dong, P. Dai, H. Zhang, X. Wang, X. Sun, S. Zhang, M. Yoon, H. Xu, Y. Ge, J. Li, F. Huang, *Nat. Energy* **2023**, *8*, 159.
[6] a) C. Lin, J. Li, Z.-W. Yin, W. Huang, Q. Zhao, Q. Weng, Q. Liu, J. Sun, G. Chen, F. Pan, *Adv. Mater.* **2023**, *n/a*, 2307404; b) J. Kikkawa, S. Terada, A. Gunji, T. Nagai, K. Kurashima, K. Kimoto, *J. Phys. Chem. C* **2015**, *119*, 15823; c) J. Gim, Y. Zhang, H. Gao, G.-L. Xu, F. Guo, Y. Ren, K. Amine, Z. Chen, *J. Power Sources* **2020**, *469*, 228422.
[7] C. Sun, X. Liao, F. Xia, Y. Zhao, L. Zhang, S. Mu, S. Shi, Y. Li, H. Peng, G. Van Tendeloo, K. Zhao, J. Wu, *ACS Nano* **2020**, *14*, 6181.
[8] a) J. Liu, J. Wang, Y. Ni, J. Liu, Y. Zhang, Y. Lu, Z. Yan, K. Zhang, Q. Zhao, F. Cheng, J. Chen, *Angew. Chem., Int. Ed.* **2022**, *61*, e202207000; b) Y. Lyu, X. Wu, K. Wang, Z. Feng, T. Cheng, Y. Liu, M. Wang, R. Chen, L. Xu, J. Zhou, Y. Lu, B. Guo, *Adv. Energy Mater.* **2020**, *11*, 2000982.
[9] a) S. Kalluri, M. Yoon, M. Jo, S. Park, S. Myeong, J. Kim, S. X. Dou, Z. Guo, J. Cho, *Adv. Energy Mater.* **2017**, *7*, 1601507; b) W. Liu, P. Oh, X. Liu, S. Myeong, W. Cho, J. Cho, *Adv. Energy Mater.* **2015**, *5*, 1500274; c) A. Fu, Z. Zhang, J. Lin, Y. Zou, C. Qin, C. Xu, P. Yan, K. Zhou, J. Hao, X. Yang, Y. Cheng, D.-Y. Wu, Y. Yang, M.-S. Wang, J. Zheng, *Energy Storage Mater.* **2022**, *46*, 406.
[10] S. Xu, X. Tan, W. Ding, W. Ren, Q. Zhao, W. Huang, J. Liu, R. Qi, Y. Zhang, J. Yang, C. Zuo, H. Ji, H. Ren, B. Cao, H. Xue, Z. Gao, H. Yi, W. Zhao, Y. Xiao, Q. Zhao, M. Zhang, F. Pan, *Angew. Chem., Int. Ed.* **2023**, *62*, e202218595.
[11] X. Tan, Y. Zhang, S. Xu, P. Yang, T. Liu, D. Mao, J. Qiu, Z. Chen, Z. Lu, F. Pan, W. Chu, *Adv. Energy Mater.* **2023**, *13*, 2300147.
[12] T. Cheng, Z. Ma, R. Qian, Y. Wang, Q. Cheng, Y. Lyu, A. Nie, B. Guo, *Adv. Funct. Mater.* **2021**, *31*, 2001974.
[13] N. Ohtsu, M. Oku, K. Satoh, K. Wagatsuma, *Appl. Surf. Sci.* **2013**, *264*, 219.
[14] H. W. Nesbitt, G. S. Henderson, G. M. Bancroft, C. O'shaughnessy, *Chem. Geol.* **2017**, *461*, 65.
[15] J. Kikkawa, S. Terada, A. Gunji, T. Nagai, K. Kurashima, K. Kimoto, *J. Phys. Chem. C* **2015**, *119*, 15823.
[16] P. Byeon, H. B. Bae, H.-S. Chung, S.-G. Lee, J.-G. Kim, H. J. Lee, J. W. Choi, S.-Y. Chung, *Adv. Funct. Mater.* **2018**, *28*, 1804564.

[17] Y. Wang, Q. Zhang, Z.-C. Xue, L. Yang, J. Wang, F. Meng, Q. Li, H. Pan, J.-N. Zhang, Z. Jiang, W. Yang, X. Yu, L. Gu, H. Li, *Adv. Energy Mater.* **2020**, *10*, 2001413.
[18] H. Yi, Y. Du, J. Fang, Z. Li, H. Ren, W. Zhao, H. Chen, L. Zhou, Q. Zhao, F. Pan, *ACS Appl. Mater. Interfaces* **2023**, *15*, 42667.
[19] J.-N. Zhang, Q. Li, Y. Wang, J. Zheng, X. Yu, H. Li, *Energy Storage Mater.* **2018**, *14*, 1.
[20] a) H. Tan, S. Takeuchi, K. K. Bharathi, I. Takeuchi, L. A. Bendersky, *ACS Appl. Mater. Interfaces* **2016**, *8*, 6727; b) R. Qin, S. Ding, C. Hou, L. Liu, Y. Wang, W. Zhao, L. Yao, Y. Shao, R. Zou, Q. Zhao, S. Li, F. Pan, *Adv. Energy Mater.* **2023**, *13*, 2203915.
[21] Z. Wu, G. Zeng, J. Yin, C.-L. Chiang, Q. Zhang, B. Zhang, J. Chen, Y. Yan, Y. Tang, H. Zhang, S. Zhou, Q. Wang, X. Kuai, Y.-G. Lin, L. Gu, Y. Qiao, S.-G. Sun, *ACS Energy Lett.* **2023**, *8*, 4806.
[22] a) Y. Kan, Y. Hu, Y. Ren, J. Bareño, I. Bloom, Y.-K. Sun, K. Amine, Z. Chen, *J. Power Sources* **2014**, *271*, 97; b) S. A. Wicker, E. H. Walker Jr., *Inorg. Chem.* **2013**, *52*, 1772; c) X. Tan, D. Mao, T. Zhao, Y. Zhang, L. Song, Z. Fan, G. Liu, H. Wang, W. Chu, *Small* **2022**, *18*, 2202143.
[23] F. Lin, I. M. Markus, D. Nordlund, T.-C. Weng, M. D. Asta, H. L. Xin, M. M. Doeff, *Nat. Commun.* **2014**, *5*, 3529.
[24] J. Qiu, X. Liu, R. Chen, Q. Li, Y. Wang, P. Chen, L. Gan, S.-J. Lee, D. Nordlund, Y. Liu, X. Yu, X. Bai, H. Li, L. Chen, *Adv. Funct. Mater.* **2020**, *30*, 1909392.
[25] J. Qian, L. Liu, J. Yang, S. Li, X. Wang, H. L. Zhuang, Y. Lu, *Nat. Commun.* **2018**, *9*, 4918.
[26] E. Hu, Q. Li, X. Wang, F. Meng, J. Liu, J.-N. Zhang, K. Page, W. Xu, L. Gu, R. Xiao, H. Li, X. Huang, L. Chen, W. Yang, X. Yu, X.-Q. Yang, *Joule* **2021**, *5*, 720.
[27] a) B. L. D. Rinkel, D. S. Hall, I. Temprano, C. P. Grey, *JACS* **2020**, *142*, 15058; b) A. L. Michan, B. S. Parimalam, M. Leskes, R. N. Kerber, T. Yoon, C. P. Grey, B. L. Lucht, *Chem. Mater.* **2016**, *28*, 8149.
[28] Z. Li, H. Yi, H. Ren, J. Fang, Y. Du, W. Zhao, H. Chen, Q. Zhao, F. Pan, *Adv. Funct. Mater.* **2023**, *33*, 2307913.
[29] Y.-C. Lu, A. N. Mansour, N. Yabuuchi, Y. Shao-Horn, *Chem. Mater.* **2009**, *21*, 4408.
[30] S. Ding, M. Zhang, R. Qin, J. Fang, H. Ren, H. Yi, L. Liu, W. Zhao, Y. Li, L. Yao, S. Li, Q. Zhao, F. Pan, *Nano-Micro Lett.* **2021**, *13*, 173.
[31] B. Zhang, L. Wang, Y. Zhang, X. Wang, Y. Qiao, S.-G. Sun, *J. Chem. Phys.* **2023**, *158*, 054202.
[32] Q. Zhao, A. Song, W. Zhao, R. Qin, S. Ding, X. Chen, Y. Song, L. Yang, H. Lin, S. Li, F. Pan, *Angew. Chem., Int. Ed.* **2021**, *60*, 4169.
[33] C. Yang, X. Liao, X. Zhou, C. Sun, R. Qu, J. Han, Y. Zhao, L. Wang, Y. You, J. Lu, *Adv. Mater.* **2023**, *35*, 2210966.